CrystEngComm

Accepted Manuscript

ROYAL SOCIETY OF CHEMISTRY

www.rsc.org/crystengcomm

Cite this: DOI: 10.1039/c0xx00000x

www.rsc.org/xxxxxx

ARTICLE TYPE

Pyrrolo[2,3-*b*]quinoxaline with 2-(2-aminoethyl)pyridine chain highly selective fluorescent receptor for Zn^{2+} exhibiting a dual fluorescence and AIEE in crystalline state

Katarzyna Ostrowska*, Łukasz Dudek, Jarosław Grolik, Marlena Gryl and Katarzyna Stadnicka‡

Received (in XXX, XXX) Xth XXXXXXXXX 20XX, Accepted Xth XXXXXXXXX 20XX
DOI: 10.1039/b000000x

The article describes the synthesis of selective dual emissive intramolecular charge transfer (ICT) receptor for zinc ion in acetonitrile, exhibiting aggregation induced emission enhancement (AIEE) in solid state due to formation of inter- or intramolecular hydrogen bonds, and aromatic donor-acceptor interaction with H- or J- aggregation.

Aggregation-caused quenching (ACQ) of light emission in solid-state is prevalent and is observed due to non-radiative decay pathway induced by intermolecular vibronic interactions such as exciton coupling and excimer formation. Solid-state organic fluorescent compounds are still exceptional. They have attracted significant attention and have been subjected to intense research because of their unique properties and potential applications as active elements in electronic and optoelectronic devices.[1] The fluorescence properties of these compounds strongly depend on their planar π-conjugated molecular structure and molecular arrangement in crystalline state. The mechanism of emission in the solid-state is attributed to two effects: aggregation induced emission (AIE)[2] or aggregation induced emission enhancement (AIEE)[3]. AIE is ascribed to the mechanism of restricted intermolecular rotational motion (RIR) and/or exciplex formation, whereas, AIEE is attributed to the synergistic combination of conformational planarization[4], H-, or J-aggregate formation[5], and hydrophobic effects. Aggregation is possible due to the formation of inter- and intramolecular hydrogen bonds and non-covalent interactions such as π – π, CH- π, CH-N, and CH-O. Molecules showing AIE and AIEE are non-emissive in organic solvent and exhibit increased fluorescence upon aggregation in the solid state or in solutions with high fractions of water.

We report herein the synthesis and photophysical properties of the new prochiral ICT[6] (*E*/*Z*)-2-(2-aminoethyl)pyridine-pyrrolo [2,3-*b*]quinoxaline derivative **2**, that exhibits turn on dual emission, selective recognition of zinc ion in solution, and spontaneous chiral resolution and racemisation induced by inter- and intramolecular hydrogen bonds formation, as well as π – π non-covalent interaction in the solid state. Coordination of zinc ion and crystallization of **2** shift *E*/*Z*-equilibrium of receptor to its *E*-form that induces rigidity and planarization of the molecule as well as increases the intramolecular charge-transfer (ICT) efficiency in solution and AIEE in the solid state.

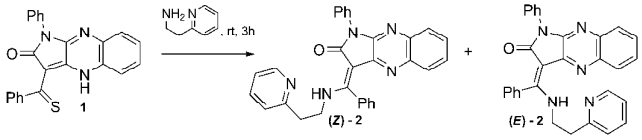

Scheme 1. *N*-Alkyl enamination of **1**.

The push-pull luminogen **2** was synthesized according to previously published enamination[7] of thioketone **1** with 2-(2-aminoethyl)pyridine (Scheme 1 and ESI). We obtained mixtures of *E*/*Z* diasteroisomers of **2** with *E*-isomer predominating in CD_3CN (4.13:1); DMSO-d_6 (4.07:1) and $CDCl_3$ (5.15:1). The temperature-dependent ^1H NMR experiment at temperature range 300-220 K in $CDCl_3$ indicated shifting (*E*/*Z*) equilibrium for **2** to *E*-form (ESI). The interconversion of *Z*-form to *E* diastereoisomer is possible due to the presence of the conjugated donor–acceptor architecture of **2** with zwitterionic resonance structures A, B, C, D and intramolecular rotations along C3 and C30 bond (Scheme 2).

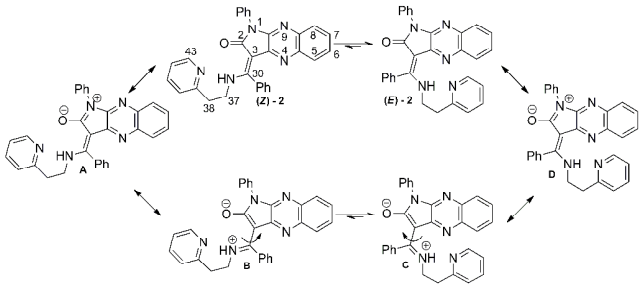

Scheme 2. Mechanism of (*Z*/*E*)-**2** interconversion.

The absorption spectrum of **2** showed two maxima (376 and 396 nm in CH_3CN, 374 and 391 nm in MeOH, 377 and 397 nm in $CHCl_3$, 377 and 398 nm, respectively) with molar absorption coefficients 23196 and 24111 $M^{-1}cm^{-1}$ in acetonitrile, which are attributed to the π – π* transitions. In hexane the new maximum

occurred at 386 nm (ESI). Both *E*/*Z* forms of **2** are not-fluorescent in acetonitrile, however, **2** exhibits luminescence at 475 nm (λ_{ex} = 420 nm) in CH_3CN-water mixture with water fractions from 50% to 70% (Fig. 1, Fig. 2, ESI). The emission enhancement is ascribed to the presence of suspension of **2** in solvent mixture.

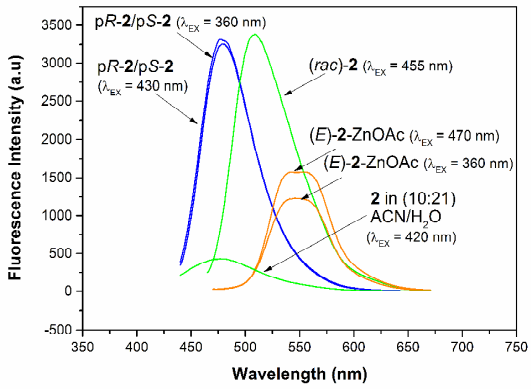

Fig. 1. Fluorescence spectra of solid (p*R*)-**2**/(p*S*)-**2** (λ_{ex}=360 and 430 nm), (*rac*)-**2**, (λ_{ex}=455 nm), **2**-ZnOAc (λ_{ex}=360 and 470 nm), and fluorescence spectra of suspension of **2** in (10:21) CH_3CN/H_2O (λ_{ex}=420 nm).

We also found that **2** responds to different metal ions with distinctive, selective dual fluorescence enhancement for zinc salts in acetonitrile (Fig. 3 and ESI). The positions of two emission bands: local excited state (LE) and intramolecular charge transfer (ICT) for **2**-ZnOAc are dependent on the solvent polarity. The LE is blue-shifted from 457 nm in $CHCl_3$, acetonitrile, and methanol to 449 nm in *n*-hexane. The ICT emission is slightly shifted to longer wavelengths: 472, 476, 476, and 478 nm in *n*-hexane, $CHCl_3$, acetonitrile, and methanol, respectively. In hexane and $CDCl_3$ the new ICT shoulder occurred at 508 and 510 nm (ESI).

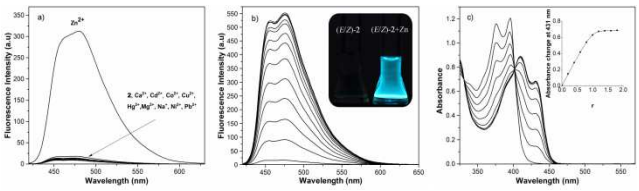

Fig. 3. (a) Fluorescence spectra of **2** (10 μM) in CH_3CN with 1 equiv. Ca^{2+}, Cd^{2+}, Co^{2+}, Cu^{2+}, Hg^{2+}, Mg^{2+}, Na^{+}, Ni^{2+}, Pb^{2+}, Zn^{2+} (λ_{ex} = 410 nm). (b) Fluorescence response upon titration of **2** (10 μM) with $Zn(OAc)_2$ (0-2 equiv.) in CH_3CN (λ_{ex} = 410 nm). Inset: Fluorescence emission of **2** solution in CH_3CN observed upon addition of 4 equiv. of $Zn(OAc)_2$ and excitation at 410 nm. (c) UV-VIS spectral titration of **2** (50 μM) with $Zn(OAc)_2$ (0-1.2 equiv.) in CH_3CN. Inset: Increase in absorbance at λ = 431 nm as a function of equiv. of Zn^{2+}.

Association constant log*K*=6.13 was estimated by fitting UV-Vis titration curve to the kinetic equation[8] of 1:1 binding equilibria using non-linear regression method (Fig. 3c, ESI).

^{1}H NMR titration showed that only (*E*)-**2** diasteroisomer coordinates zinc ion simultaneously with deprotonation. Formation of (*E*)-**2-ZnOAc** complex with binding mode 1:1 imposes isomerisation of (*Z*)-**2** to its *E*-form during the addition of zinc ion, shifting *E*/*Z* equilibrium in acetonitrile (ESI). The coordination of metal ion stiffened and flattened the molecule as well as restricts the intramolecular rotation of the C3 and C30 bond in the solution.

We found that in the 50% water-acetonitrile solution compound **2** crystallizes in emissive racemic form (*rac*)-**2** (Figs 1, 2, ESI). The X-ray crystal structure analysis (ESI: Table 1) revealed that the crystals of (*rac*)-**2** are built of two symmetrically independent molecules shown in Fig. 4a-b with the same planar chirality p*R* but with conformations of 2-ethyl-pyrididine group **A** and **B**, respectively (ESI: Table 2, Figs 6.1.1-4). Following the space group symmetry Cc the structure contains both p*R* and p*S* stereoisomers (racemate).

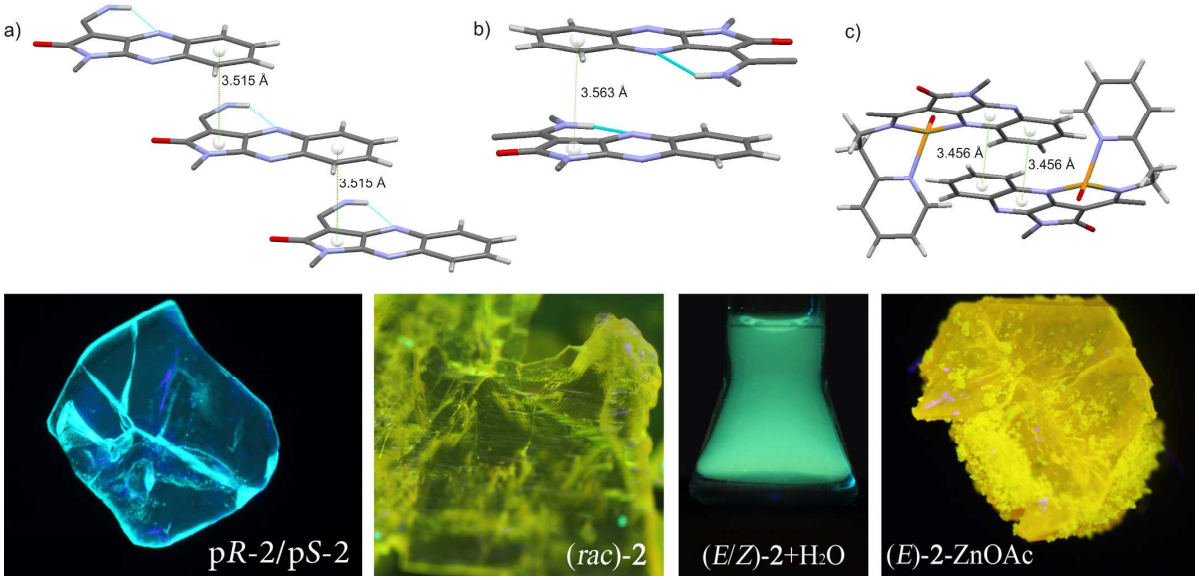

Fig.2. (a), (b), (c) π-π Interaction between planar fluorophores in crystal structure of (p*R*)-**2**/(p*S*)-**2**, (*rac*)-**2**, **2**-ZnOAc. Bottom: photographs of the crystals: (p*R*)-**2**/(p*S*)-**2**, (*rac*)-**2**, **2**-ZnOAc (λ_{ex} = 410 nm, diode UV), and suspension of (*E*/*Z*)-**2** in CH_3CN-water mixture with water fractions 67% in cuvette (λ_{ex} = 365 nm, hand-held UV lamp).

Cite this: DOI: 10.1039/c0xx00000x

www.rsc.org/xxxxxx

ARTICLE TYPE

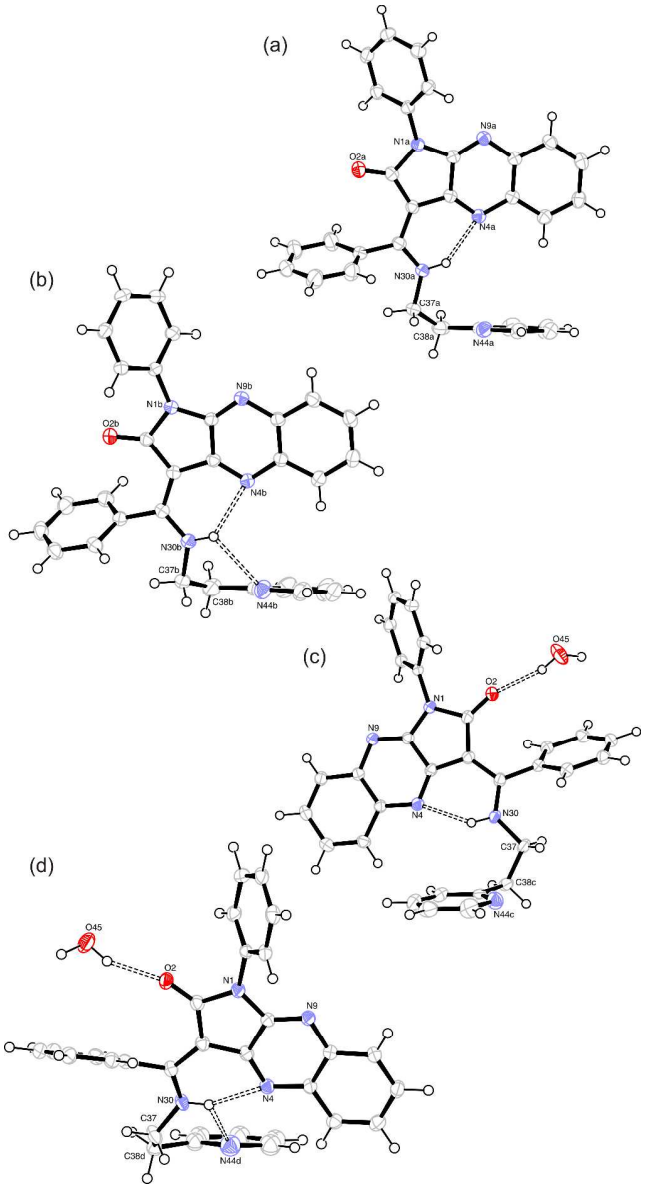

Fig. 4. (rac)-**2**: Symmetrically independent molecules of p*R* configuration (C37 is the pilot atom) and conformations A (a) and B (b) of ethyl pyridine moiety. (p*S*)-**2**/(p*R*)-**2**: Molecule of pS configuration and C conformation with site occupancy factor 0.828 (c) and that of pR configuration and D conformation with site occupancy factor 0.172 (d). The non-hydrogen atoms are represented as displacement ellipsoids at 50 % probability level.

The conformation **A** is stabilized by N(30A)-H(30A)…N(44A) hydrogen bond, 2.05(2) Å, whereas, **B** conformation is stabilized by intramolecular bifurcated hydrogen bond: N(30B)-H(30B) to N(4B) and to N(44B) (2.22(2) Å and 2.42(2) Å, respectively (ESI: Table 3).

A and **B** are related by the strong π-π interaction between pyrrolo[2,3-*b*]quinoxaline fused systems with head to tail fashion following J-aggregation[6] and the interlayer distance between adjacent fluorophores 3.397 Å. (Fig. 2b, ESI: Table 3).

Addition of several water drops during crystallization of **2** from acetonitrile resulted also in formation of the pair of enantiomers (p*R*)-**2** and (p*S*)-**2** with two 2-ethylpyridine chain conformations **C** and **D** (Fig.2a, Figs 4c-d). We found that water molecules assemble two crystal framework with helical arrangements along the *b* – axis within the space group $P2_1$. The structure is mainly formed by the water molecules spontaneously linked through H-bonds with two acceptors: oxygen of carbonyl group and nitrogen atom of pyridyl group from two ligand molecules related by symmetry (C=O···H-O-H, 2.809(2) Å; H-O-H···N-Py; 2.969(2) Å, ESI: Table 3, Figs 6.2.1-4). We obtained crystals of both enantiomers in the same crystallization process, which was proved by X-ray analyses. Isolated crystal with determined absolute structure, Flack parameter = 0.0(2), contains 82.8(4)% of (p*S*)-**2** with **C** conformation and 17.2(4) % of (p*R*)-**2** with **D** conformation (Figs 4c-d, ESI: Table 2). Intermolecular multiple hydrogen bonds stiffen molecular conformation. Furthermore, the water molecules in crystalline state facilitate formation of π-π interactions (3.406 Å) between pyrrolo[2,3-*b*]quinoxaline fused systems with cofacial fashion (H-aggregation) and change the fluorophore arrangement in the solid state in contrast to crystal structure of (*rac*)-**2**.

The π-π overlap between adjacent molecules increases interplanar distance that changes optical and electronic properties of (p*R*)-**2**/(p*S*)-**2** that result in blue-shifted fluorescence emission (shift of 31 nm; λ_{ex}/ λ_{em} = 430/474 nm) with respect to (*rac*)-**2** for the solid state (Fig. 1, Fig. 2).

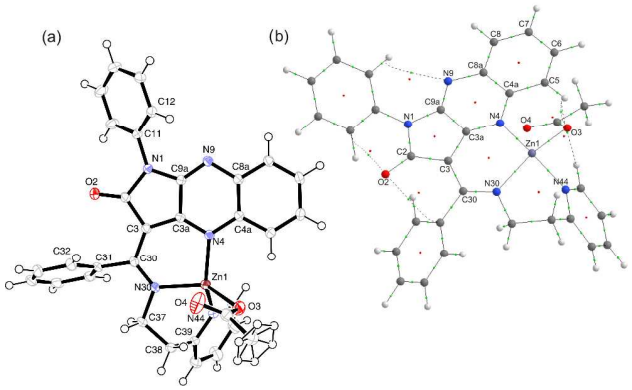

Fig. 5. (a) **2-ZnOAc** with zinc atom as stereogenic centre (note that the crystal structure is centrosymmetric, space group $P2_1/c$, so it contains both enantiomers). The non-hydrogen atoms are represented as displacement ellipsoids at 50 % probability level. (b) Molecular graph of **2-ZnOAc** with bond (3,-1) and ring (3, +1) critical points as green and red spheres, respectively.

In both cases, (*rac*)-**2** and (p*S*)-**2**/(p*R*)-**2,** we observed crystallization induced emission enhancement (CIE) only for (*E*)-**2** diastereoisomer.

Isolated complex of (*E*)-**2-ZnOAc** exhibits a distorted tetrahedral structure in which the nitrogen (N4, N30, N44), and oxygen donors coordinate to zinc (Fig. 5a, ESI: Table 2, Figs 6.3.1-4). The X-ray analysis of single crystals (*E*)-**2-ZnOAc** also showed the strong π-π interaction between pyrrolo[2,3-*b*]quinoxaline fused systems with head to tail fashion (J-aggregation) and interlayer distance between the adjacent molecular fluorophores 3.353 Å (Fig.2c, ESI: Table 3). It was to note, that the crystal structure is assembled due to interactions with two acetonitrile molecules of opposite alignment of one dipole with the other (ESI: 6.3.3). These interactions change optical and electronic properties of (*E*)-**2-ZnOAc** and results in red-shifted dual fluorescence emission ($\lambda_{ex}/\lambda_{em}$ = 470/543 nm, 470/552 nm) for solid state (Fig. 1, Fig. 2.). The fluorescence spectra of **2-ZnOAc** in solid state exhibit two maxima for the complex. Single crystal X-ray and powder X-ray diffraction (PXRD) analyses of **2-ZnOAc** confirmed the presence exclusively one crystal form in sample (ESI: Fig 6.3.5).

QTAIM analysis of charge density for (*E*)-**2-ZnOAc** (AIMAll[10]), and analysis of energetic criteria based on local potential and kinetic energy density allowed to classify the Zn-O3, Zn-N4, Zn-N30, and Zn-N4 bonds as intermediate between closed shell and shared shell interaction (|V(rCP)|/G(rCP) in the range between 1 and 2; E(rCP) / r(r) <0). As expected the Zn1-O3 interaction has more pronounced closed shell character comparing to the Zn-N bonds as seen by the more positive value of Laplacian at BCP (Fig. 5b, ESI: Tables 4). QTAIM net atomic charges were calculated for the selected atoms (Table 5: ESI) and show +1.26 charge on the Zn ion, which is an integral part of donor group and increases π-conjugation in coplanar push-pull system with amide carbonyl group as acceptor.

The presence of dual fluorescence of (*E*)-**2-ZnOAc** in the solution may be a consequence of planar intramolecular charge transfer (PICT)[9] state due to inhibition of *E*/*Z*-isomerisation and twisted intramolecular charge transfer (TICT) state due to the presence of secondary amino group in enamine moiety. The PICT model postulates formation of the highly polar planar quinoid ICT structure with an increased double bond character between the donor and acceptor moieties as well as partial positive charge on the amino group. X-ray analysis of (*pS*)-**2**/(*pR*)-**2**, (rac)-**2** for ligands and (*E*)-**2-ZnOAc** confirmed the prevalence of the partial double character of C30-N30 bond for ligands: 1.327-1.330 Å, responsible for *Z*/*E* isomerisation of **2** (Scheme 2) and double bond for (*E*)-**2-ZnOAc** (1.309 Å). It should be noted, that the origin of dual emission requires further explanation and more detailed studies, which are in progress.

Conclusions

We have described a new class of ICT turn on, dual-emissive, ratiometric receptor for zinc ion in solution. We determined that donor-acceptor conjugated pyrroloquinoxaline **2** exhibits chiral spontaneous resolution and racemisation by inter- and intramolecular hydrogen bond formation, as well as π – π non-covalent interaction in the solid state. Enhanced fluorescence emission of pyrroloquinoxaline derivatives was attributed to the synergic effect of planarization and coordination of zinc ion in solution and additional H-, or J-aggregation in the solid state.

Notes and references

*Faculty of Chemistry, Jagiellonian University, R. Ingardena 3, PL-30-060 Kraków, Poland. E-mail ostrowsk@chemia.uj.edu.pl; Fax: +48-12 63-40-515

†Electronic Supplementary Information (ESI) available: [Synthetic procedure, temperature-dependent ^{1}H NMR spectra, ^{1}H NMR spectra upon titration with Zn(OAc)$_2$, 1D and 2D fluorescence spectra, absorption spectra, crystallographic data, topological analyses, DFT calculation. CCDC 1006387, CCDC 1006388, CCDC 1006389. See DOI: 10.1039/b000000x

‡For crystal structure information, E-mail: stadnick@chemia.uj.edu.pl

The Authors would like to thank dr Marcin Kozieł for performing PXRD measurement. The research was carried out with the equipment purchased thanks to the financial support of the European Regional Development Fund in the framework of the Polish Innovation Economy Operational Program (contract no. POIG.02.01.00-12-023/08). This research was supported in part by PL-Grid Infrastructure.

1 Y. S. Zhao, H. Fu, A. Peng, Y. Ma, Q. Liao, J.Yao, *Acc Chem. Res.,* 2010, **43**, 409**;** H. Xu, R. Chen, Q. Sun, W. Lai, Q. Su, W. Huang, X. Liu, *Chem. Soc. Rev.*, 2014, **43**, 3259**;** M. Zhu, Ch. Yang, *Chem. Soc. Rev.* 2013, **42**, 4963**;** X. Zhao, X. Zhan, *Chem. Soc. Rev.* 2011, **40**, 3728.

2 Y. Hong, J. W. Y. Lam, B. Zh. Tang, *Chem. Comm.,* 2009, **45**, 4332; Y. Hong, J. W. Y. Lam, B. Zh. Tang, *Chem. Soc. Rev.,* 2011, **40**, 5361; Z. Zhao, B. He, H. Nie, B. Chen, P. Lu, A. Qin, B. Zh. Tang, *Chem. Comm.,* 2014, **50**, 1131; R. Hu, Sh. Li, Y. Zeng, J. Chen, Sh. Wang, Y. Li, G. Yang, *Phys. Chem. Chem. Phys.*, 2011, **13**, 2044; E. P. J. Parrott, N. Y. Tan, R. Hu, J. A. Zeitler, B. Zh. Tang and E. Pickwell-MacPherson, *Mater. Horiz.*, 2014, **1**, 251.

3 S.-J. Yoon, J. W. Chung, J. Gierschner, K. S. Kim, M.-G. Choi, D. Kim, S. Y. Park, *J. Am. Chem. Soc.*, 2010, **132**, 13675; M. Cai, Zh. Gao, X. Zhou, X. Wang, Sh. Chen, Y. Zhao, Y. Qian, N. Shi, B. Mi, L. Xie, W. Huang, *Phys. Chem. Chem. Phys.*, 2012, **14**, 5289; B.-K. An, J. Gierschner, S. Y. Park, *Acc. Chem. Res.*, 2012, **45**, 544; Q. Dai, W. Liu, L. Zeng, Ch.-S. Lee, J. Wu, P. Wang, *CrystEngComm*, 2011, **13**, 4617; N. Komiya, N. Itami, T. Naota, *Chem. Eur. J.* 2013, **19**, 9497; T. He, X.-T. Tao, J.-X. Yang, D. Guo, H.-B. Xia, J. Jia, M.-H. Jiang, *Chem. Comm.,* 2011, **47**, 2907;

4 B.-K. An, S.-K. Kwon, S.-D. Jung, S. Y. Park, *J. Am. Chem. Soc.*, 2002, **124**, 14410.

5 Sh. Varghese, S. Das, *J. Phys. Chem. Lett.*, 2011,**2**, 863; D. Yan, D. G. Evans, *Mater. Horiz.*, 2014, **1**, 46; J. Gierschner, S. Y. Park, *J. Mater. Chem. C.*, 2013, **1**, 5818.

6 Y. Li, T. Liu, H. Liu, M.-Zh. Tian, Y. Li, *Acc Chem. Res.,* 2014, **47**, 1186.

7 K. Ostrowska, E. Piegza, M. Rąpała-Kozik, K. Stadnicka, *Eur. J. Org. Chem*., 2012,**19**, 3636; K. Ostrowska, A. Kaźmierska, M. Rąpała-Kozik, and J. Kalinowska-Tłuścik, *New J. Chem.*, 2014, **38**, 213.

8 P. Thordason, *Chem. Soc. Rev*., 2011, **40**, 1305; P. Thordason, *Chem. Soc. Rev*., 2011, **40**, 5922.

9 K. A. Zachariasse, M. Grobys, Th. von der Haar, A. Hebecker, Yu. V. Il'ichev, O. Morawski, I. Rückert, W. Kühnie, *J. Photochem. Photobiol. A: Chem.*, 1997, **105**, 373; K. A. Zachariasse, *Chem. Phys. Lett.*, 2000, **320**, 8; Z. R. Grabowski, K. Rotkiewicz, W. Rettig, *Chem. Rev.*, 2003, **103**, 899; C. A. Guido, B. Mennucci, D. Jacquemin, and C. Adamo, *Phys. Chem. Chem. Phys.*, 2010, **12**, 8016.

10 T. A. Keith (2010). AIMAII program (Version 10.11.24). aim.tkgristmill.com.

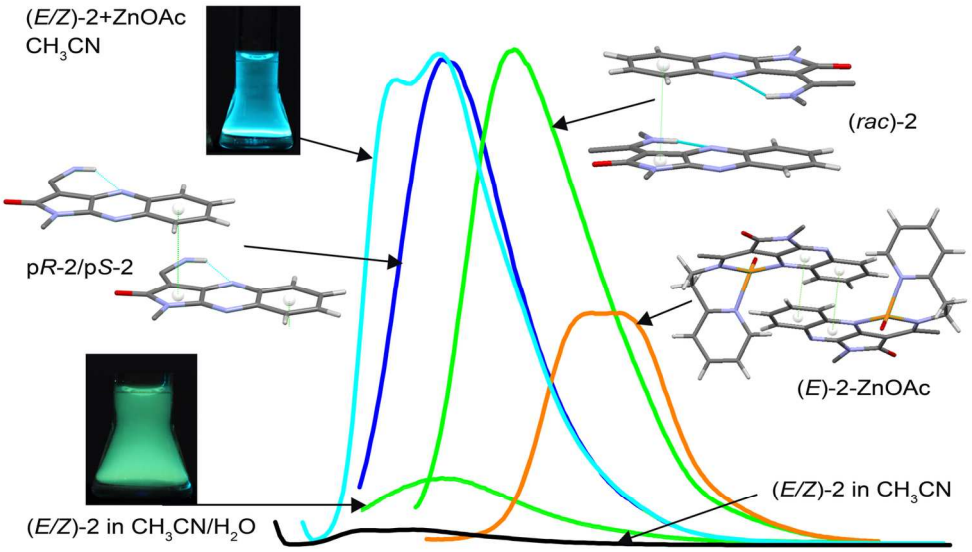

149x93mm (300 x 300 DPI)